BABAR-CONF-04/043
SLAC-PUB-10637
December 2004

arXiv:hep-ex/0408088v2 15 Dec 2004

Constraints on r_B and γ in $B^{\pm} \to D^{(*)0}K^{\pm}$ decays by a Dalitz analysis of $D^0 \to K_S\pi^-\pi^+$

The *BABAR* Collaboration

February 7, 2008

Abstract

We report on a study of direct CP violation in the decay $B^- \to D^{(*)0}K^-$ with a Dalitz analysis of the $D^0 \to K_S\pi^-\pi^+$ decay using a sample of 227 million $B\overline{B}$ pairs collected by the *BABAR* detector. Reference to the charge-conjugate state is implied here. We constrain the amplitude ratio $r_B = \frac{|A(B^- \to \overline{D}^0 K^-)|}{|A(B^- \to D^0 K^-)|}$ to be < 0.19 at the 90% confidence level and $r_B^* = \frac{|A(B^- \to \overline{D}^{*0} K^-)|}{|A(B^- \to D^{*0} K^-)|} = 0.155^{+0.070}_{-0.077} \pm 0.040 \pm 0.020$ and we measure the relative strong phase $\delta_B = (114 \pm 41 \pm 8 \pm 10)^\circ$ and $\delta_B^* = (303 \pm 34 \pm 14 \pm 10)^\circ$ between the amplitudes $A(B^- \to \overline{D}^{(*)0} K^-)$ and $A(B^- \to D^{(*)0} K^-)$. From these samples we measure $\gamma = (70 \pm 26 \pm 10 \pm 10)^\circ$. The first error is statistical, the second error accounts for experimental uncertainties and the third error reflects the Dalitz model uncertainty. For this preliminary result we have quoted confidence intervals obtained with a Bayesian technique assuming a uniform prior in r_B, γ and δ_B.

Submitted to the 32nd International Conference on High-Energy Physics, ICHEP 04, 16 August—22 August 2004, Beijing, China

Stanford Linear Accelerator Center, Stanford University, Stanford, CA 94309

Work supported in part by Department of Energy contract DE-AC03-76SF00515.

The *BABAR* Collaboration,

B. Aubert, R. Barate, D. Boutigny, F. Couderc, J.-M. Gaillard, A. Hicheur, Y. Karyotakis, J. P. Lees, V. Tisserand, A. Zghiche

Laboratoire de Physique des Particules, F-74941 Annecy-le-Vieux, France

A. Palano, A. Pompili

Università di Bari, Dipartimento di Fisica and INFN, I-70126 Bari, Italy

J. C. Chen, N. D. Qi, G. Rong, P. Wang, Y. S. Zhu

Institute of High Energy Physics, Beijing 100039, China

G. Eigen, I. Ofte, B. Stugu

University of Bergen, Inst. of Physics, N-5007 Bergen, Norway

G. S. Abrams, A. W. Borgland, A. B. Breon, D. N. Brown, J. Button-Shafer, R. N. Cahn, E. Charles, C. T. Day, M. S. Gill, A. V. Gritsan, Y. Groysman, R. G. Jacobsen, R. W. Kadel, J. Kadyk, L. T. Kerth, Yu. G. Kolomensky, G. Kukartsev, G. Lynch, L. M. Mir, P. J. Oddone, T. J. Orimoto, M. Pripstein, N. A. Roe, M. T. Ronan, V. G. Shelkov, W. A. Wenzel

Lawrence Berkeley National Laboratory and University of California, Berkeley, CA 94720, USA

M. Barrett, K. E. Ford, T. J. Harrison, A. J. Hart, C. M. Hawkes, S. E. Morgan, A. T. Watson

University of Birmingham, Birmingham, B15 2TT, United Kingdom

M. Fritsch, K. Goetzen, T. Held, H. Koch, B. Lewandowski, M. Pelizaeus, M. Steinke

Ruhr Universität Bochum, Institut für Experimentalphysik 1, D-44780 Bochum, Germany

J. T. Boyd, N. Chevalier, W. N. Cottingham, M. P. Kelly, T. E. Latham, F. F. Wilson

University of Bristol, Bristol BS8 1TL, United Kingdom

T. Cuhadar-Donszelmann, C. Hearty, N. S. Knecht, T. S. Mattison, J. A. McKenna, D. Thiessen

University of British Columbia, Vancouver, BC, Canada V6T 1Z1

A. Khan, P. Kyberd, L. Teodorescu

Brunel University, Uxbridge, Middlesex UB8 3PH, United Kingdom

A. E. Blinov, V. E. Blinov, V. P. Druzhinin, V. B. Golubev, V. N. Ivanchenko, E. A. Kravchenko, A. P. Onuchin, S. I. Serednyakov, Yu. I. Skovpen, E. P. Solodov, A. N. Yushkov

Budker Institute of Nuclear Physics, Novosibirsk 630090, Russia

D. Best, M. Bruinsma, M. Chao, I. Eschrich, D. Kirkby, A. J. Lankford, M. Mandelkern, R. K. Mommsen, W. Roethel, D. P. Stoker

University of California at Irvine, Irvine, CA 92697, USA

C. Buchanan, B. L. Hartfiel

University of California at Los Angeles, Los Angeles, CA 90024, USA

S. D. Foulkes, J. W. Gary, B. C. Shen, K. Wang

University of California at Riverside, Riverside, CA 92521, USA

D. del Re, H. K. Hadavand, E. J. Hill, D. B. MacFarlane, H. P. Paar, Sh. Rahatlou, V. Sharma

University of California at San Diego, La Jolla, CA 92093, USA

J. W. Berryhill, C. Campagnari, B. Dahmes, O. Long, A. Lu, M. A. Mazur, J. D. Richman, W. Verkerke

University of California at Santa Barbara, Santa Barbara, CA 93106, USA

T. W. Beck, A. M. Eisner, C. A. Heusch, J. Kroseberg, W. S. Lockman, G. Nesom, T. Schalk, B. A. Schumm, A. Seiden, P. Spradlin, D. C. Williams, M. G. Wilson

University of California at Santa Cruz, Institute for Particle Physics, Santa Cruz, CA 95064, USA

J. Albert, E. Chen, G. P. Dubois-Felsmann, A. Dvoretskii, D. G. Hitlin, I. Narsky, T. Piatenko, F. C. Porter, A. Ryd, A. Samuel, S. Yang

California Institute of Technology, Pasadena, CA 91125, USA

S. Jayatilleke, G. Mancinelli, B. T. Meadows, M. D. Sokoloff

University of Cincinnati, Cincinnati, OH 45221, USA

T. Abe, F. Blanc, P. Bloom, S. Chen, W. T. Ford, U. Nauenberg, A. Olivas, P. Rankin, J. G. Smith, J. Zhang, L. Zhang

University of Colorado, Boulder, CO 80309, USA

A. Chen, J. L. Harton, A. Soffer, W. H. Toki, R. J. Wilson, Q. Zeng

Colorado State University, Fort Collins, CO 80523, USA

D. Altenburg, T. Brandt, J. Brose, M. Dickopp, E. Feltresi, A. Hauke, H. M. Lacker, R. Müller-Pfefferkorn, R. Nogowski, S. Otto, A. Petzold, J. Schubert, K. R. Schubert, R. Schwierz, B. Spaan, J. E. Sundermann

Technische Universität Dresden, Institut für Kern- und Teilchenphysik, D-01062 Dresden, Germany

D. Bernard, G. R. Bonneaud, F. Brochard, P. Grenier, S. Schrenk, Ch. Thiebaux, G. Vasileiadis, M. Verderi

Ecole Polytechnique, LLR, F-91128 Palaiseau, France

D. J. Bard, P. J. Clark, D. Lavin, F. Muheim, S. Playfer, Y. Xie

University of Edinburgh, Edinburgh EH9 3JZ, United Kingdom

M. Andreotti, V. Azzolini, D. Bettoni, C. Bozzi, R. Calabrese, G. Cibinetto, E. Luppi, M. Negrini, L. Piemontese, A. Sarti

Università di Ferrara, Dipartimento di Fisica and INFN, I-44100 Ferrara, Italy

E. Treadwell

Florida A&M University, Tallahassee, FL 32307, USA

F. Anulli, R. Baldini-Ferroli, A. Calcaterra, R. de Sangro, G. Finocchiaro, P. Patteri, I. M. Peruzzi, M. Piccolo, A. Zallo

Laboratori Nazionali di Frascati dell'INFN, I-00044 Frascati, Italy

A. Buzzo, R. Capra, R. Contri, G. Crosetti, M. Lo Vetere, M. Macri, M. R. Monge, S. Passaggio, C. Patrignani, E. Robutti, A. Santroni, S. Tosi

Università di Genova, Dipartimento di Fisica and INFN, I-16146 Genova, Italy

S. Bailey, G. Brandenburg, K. S. Chaisanguanthum, M. Morii, E. Won

Harvard University, Cambridge, MA 02138, USA

R. S. Dubitzky, U. Langenegger

Universität Heidelberg, Physikalisches Institut, Philosophenweg 12, D-69120 Heidelberg, Germany

W. Bhimji, D. A. Bowerman, P. D. Dauncey, U. Egede, J. R. Gaillard, G. W. Morton, J. A. Nash, M. B. Nikolich, G. P. Taylor

Imperial College London, London, SW7 2AZ, United Kingdom

M. J. Charles, G. J. Grenier, U. Mallik

University of Iowa, Iowa City, IA 52242, USA

J. Cochran, H. B. Crawley, J. Lamsa, W. T. Meyer, S. Prell, E. I. Rosenberg, A. E. Rubin, J. Yi

Iowa State University, Ames, IA 50011-3160, USA

M. Biasini, R. Covarelli, M. Pioppi

Università di Perugia, Dipartimento di Fisica and INFN, I-06100 Perugia, Italy

M. Davier, X. Giroux, G. Grosdidier, A. Höcker, S. Laplace, F. Le Diberder, V. Lepeltier, A. M. Lutz, T. C. Petersen, S. Plaszczynski, M. H. Schune, L. Tantot, G. Wormser

Laboratoire de l'Accélérateur Linéaire, F-91898 Orsay, France

C. H. Cheng, D. J. Lange, M. C. Simani, D. M. Wright

Lawrence Livermore National Laboratory, Livermore, CA 94550, USA

A. J. Bevan, C. A. Chavez, J. P. Coleman, I. J. Forster, J. R. Fry, E. Gabathuler, R. Gamet, D. E. Hutchcroft, R. J. Parry, D. J. Payne, R. J. Sloane, C. Touramanis

University of Liverpool, Liverpool L69 72E, United Kingdom

J. J. Back,[1] C. M. Cormack, P. F. Harrison,[1] F. Di Lodovico, G. B. Mohanty[1]

Queen Mary, University of London, E1 4NS, United Kingdom

C. L. Brown, G. Cowan, R. L. Flack, H. U. Flaecher, M. G. Green, P. S. Jackson, T. R. McMahon, S. Ricciardi, F. Salvatore, M. A. Winter

University of London, Royal Holloway and Bedford New College, Egham, Surrey TW20 0EX, United Kingdom

D. Brown, C. L. Davis

University of Louisville, Louisville, KY 40292, USA

J. Allison, N. R. Barlow, R. J. Barlow, P. A. Hart, M. C. Hodgkinson, G. D. Lafferty, A. J. Lyon, J. C. Williams

University of Manchester, Manchester M13 9PL, United Kingdom

A. Farbin, W. D. Hulsbergen, A. Jawahery, D. Kovalskyi, C. K. Lae, V. Lillard, D. A. Roberts

University of Maryland, College Park, MD 20742, USA

G. Blaylock, C. Dallapiccola, K. T. Flood, S. S. Hertzbach, R. Kofler, V. B. Koptchev, T. B. Moore, S. Saremi, H. Staengle, S. Willocq

University of Massachusetts, Amherst, MA 01003, USA

[1]Now at Department of Physics, University of Warwick, Coventry, United Kingdom

R. Cowan, G. Sciolla, S. J. Sekula, F. Taylor, R. K. Yamamoto

Massachusetts Institute of Technology, Laboratory for Nuclear Science, Cambridge, MA 02139, USA

D. J. J. Mangeol, P. M. Patel, S. H. Robertson

McGill University, Montréal, QC, Canada H3A 2T8

A. Lazzaro, V. Lombardo, F. Palombo

Università di Milano, Dipartimento di Fisica and INFN, I-20133 Milano, Italy

J. M. Bauer, L. Cremaldi, V. Eschenburg, R. Godang, R. Kroeger, J. Reidy, D. A. Sanders, D. J. Summers, H. W. Zhao

University of Mississippi, University, MS 38677, USA

S. Brunet, D. Côté, P. Taras

Université de Montréal, Laboratoire René J. A. Lévesque, Montréal, QC, Canada H3C 3J7

H. Nicholson

Mount Holyoke College, South Hadley, MA 01075, USA

N. Cavallo,[2] F. Fabozzi,[2] C. Gatto, L. Lista, D. Monorchio, P. Paolucci, D. Piccolo, C. Sciacca

Università di Napoli Federico II, Dipartimento di Scienze Fisiche and INFN, I-80126, Napoli, Italy

M. Baak, H. Bulten, G. Raven, H. L. Snoek, L. Wilden

NIKHEF, National Institute for Nuclear Physics and High Energy Physics, NL-1009 DB Amsterdam, The Netherlands

C. P. Jessop, J. M. LoSecco

University of Notre Dame, Notre Dame, IN 46556, USA

T. Allmendinger, K. K. Gan, K. Honscheid, D. Hufnagel, H. Kagan, R. Kass, T. Pulliam, A. M. Rahimi, R. Ter-Antonyan, Q. K. Wong

Ohio State University, Columbus, OH 43210, USA

J. Brau, R. Frey, O. Igonkina, C. T. Potter, N. B. Sinev, D. Strom, E. Torrence

University of Oregon, Eugene, OR 97403, USA

F. Colecchia, A. Dorigo, F. Galeazzi, M. Margoni, M. Morandin, M. Posocco, M. Rotondo, F. Simonetto, R. Stroili, G. Tiozzo, C. Voci

Università di Padova, Dipartimento di Fisica and INFN, I-35131 Padova, Italy

M. Benayoun, H. Briand, J. Chauveau, P. David, Ch. de la Vaissière, L. Del Buono, O. Hamon, M. J. J. John, Ph. Leruste, J. Malcles, J. Ocariz, M. Pivk, L. Roos, S. T'Jampens, G. Therin

Universités Paris VI et VII, Laboratoire de Physique Nucléaire et de Hautes Energies, F-75252 Paris, France

P. F. Manfredi, V. Re

Università di Pavia, Dipartimento di Elettronica and INFN, I-27100 Pavia, Italy

[2]Also with Università della Basilicata, Potenza, Italy

P. K. Behera, L. Gladney, Q. H. Guo, J. Panetta

University of Pennsylvania, Philadelphia, PA 19104, USA

C. Angelini, G. Batignani, S. Bettarini, M. Bondioli, F. Bucci, G. Calderini, M. Carpinelli, F. Forti, M. A. Giorgi, A. Lusiani, G. Marchiori, F. Martinez-Vidal,[3] M. Morganti, N. Neri, E. Paoloni, M. Rama, G. Rizzo, F. Sandrelli, J. Walsh

Università di Pisa, Dipartimento di Fisica, Scuola Normale Superiore and INFN, I-56127 Pisa, Italy

M. Haire, D. Judd, K. Paick, D. E. Wagoner

Prairie View A&M University, Prairie View, TX 77446, USA

N. Danielson, P. Elmer, Y. P. Lau, C. Lu, V. Miftakov, J. Olsen, A. J. S. Smith, A. V. Telnov

Princeton University, Princeton, NJ 08544, USA

F. Bellini, G. Cavoto,[4] R. Faccini, F. Ferrarotto, F. Ferroni, M. Gaspero, L. Li Gioi, M. A. Mazzoni, S. Morganti, M. Pierini, G. Piredda, F. Safai Tehrani, C. Voena

Università di Roma La Sapienza, Dipartimento di Fisica and INFN, I-00185 Roma, Italy

S. Christ, G. Wagner, R. Waldi

Universität Rostock, D-18051 Rostock, Germany

T. Adye, N. De Groot, B. Franek, N. I. Geddes, G. P. Gopal, E. O. Olaiya

Rutherford Appleton Laboratory, Chilton, Didcot, Oxon, OX11 0QX, United Kingdom

R. Aleksan, S. Emery, A. Gaidot, S. F. Ganzhur, P.-F. Giraud, G. Hamel de Monchenault, W. Kozanecki, M. Legendre, G. W. London, B. Mayer, G. Schott, G. Vasseur, Ch. Yèche, M. Zito

DSM/Dapnia, CEA/Saclay, F-91191 Gif-sur-Yvette, France

M. V. Purohit, A. W. Weidemann, J. R. Wilson, F. X. Yumiceva

University of South Carolina, Columbia, SC 29208, USA

D. Aston, R. Bartoldus, N. Berger, A. M. Boyarski, O. L. Buchmueller, R. Claus, M. R. Convery, M. Cristinziani, G. De Nardo, D. Dong, J. Dorfan, D. Dujmic, W. Dunwoodie, E. E. Elsen, S. Fan, R. C. Field, T. Glanzman, S. J. Gowdy, T. Hadig, V. Halyo, C. Hast, T. Hryn'ova, W. R. Innes, M. H. Kelsey, P. Kim, M. L. Kocian, D. W. G. S. Leith, J. Libby, S. Luitz, V. Luth, H. L. Lynch, H. Marsiske, R. Messner, D. R. Muller, C. P. O'Grady, V. E. Ozcan, A. Perazzo, M. Perl, S. Petrak, B. N. Ratcliff, A. Roodman, A. A. Salnikov, R. H. Schindler, J. Schwiening, G. Simi, A. Snyder, A. Soha, J. Stelzer, D. Su, M. K. Sullivan, J. Va'vra, S. R. Wagner, M. Weaver, A. J. R. Weinstein, W. J. Wisniewski, M. Wittgen, D. H. Wright, A. K. Yarritu, C. C. Young

Stanford Linear Accelerator Center, Stanford, CA 94309, USA

P. R. Burchat, A. J. Edwards, T. I. Meyer, B. A. Petersen, C. Roat

Stanford University, Stanford, CA 94305-4060, USA

S. Ahmed, M. S. Alam, J. A. Ernst, M. A. Saeed, M. Saleem, F. R. Wappler

State University of New York, Albany, NY 12222, USA

[3]Also with IFIC, Instituto de Física Corpuscular, CSIC-Universidad de Valencia, Valencia, Spain
[4]Also with Princeton University, Princeton, USA

W. Bugg, M. Krishnamurthy, S. M. Spanier
University of Tennessee, Knoxville, TN 37996, USA

R. Eckmann, H. Kim, J. L. Ritchie, A. Satpathy, R. F. Schwitters
University of Texas at Austin, Austin, TX 78712, USA

J. M. Izen, I. Kitayama, X. C. Lou, S. Ye
University of Texas at Dallas, Richardson, TX 75083, USA

F. Bianchi, M. Bona, F. Gallo, D. Gamba
Università di Torino, Dipartimento di Fisica Sperimentale and INFN, I-10125 Torino, Italy

L. Bosisio, C. Cartaro, F. Cossutti, G. Della Ricca, S. Dittongo, S. Grancagnolo, L. Lanceri, P. Poropat,[5] L. Vitale, G. Vuagnin
Università di Trieste, Dipartimento di Fisica and INFN, I-34127 Trieste, Italy

R. S. Panvini
Vanderbilt University, Nashville, TN 37235, USA

Sw. Banerjee, C. M. Brown, D. Fortin, P. D. Jackson, R. Kowalewski, J. M. Roney, R. J. Sobie
University of Victoria, Victoria, BC, Canada V8W 3P6

H. R. Band, B. Cheng, S. Dasu, M. Datta, A. M. Eichenbaum, M. Graham, J. J. Hollar, J. R. Johnson, P. E. Kutter, H. Li, R. Liu, A. Mihalyi, A. K. Mohapatra, Y. Pan, R. Prepost, P. Tan, J. H. von Wimmersperg-Toeller, J. Wu, S. L. Wu, Z. Yu
University of Wisconsin, Madison, WI 53706, USA

M. G. Greene, H. Neal
Yale University, New Haven, CT 06511, USA

[5]Deceased

1 INTRODUCTION

In the past years CP violation in the B meson system has been clearly established [1] and although there is good agreement with the expectations of the Standard Model, further measurements of CP violation in B decays are needed to over-constrain the unitarity triangle and look for New Physics effects. A crucial test will be represented by the measurement of γ, which is the complex phase of the Cabibbo-Kobayashi-Maskawa [2] quark mixing matrix element V_{ub} in the Wolfenstein parameterization [3].
Various methods using $B^- \to D^0 K^-$ decays [4] have been proposed to measure the unitarity triangle angle γ, all exploiting the fact that a B^- can decay into a $D^0 K^-$ final state via a $b \to c$ transition or into a $\overline{D}^0 K^-$ final state via a $b \to u$ transition. CP violation can be detected if the D^0 and $\overline{D}^0$ decay into the same final state. The measurement of direct CP violation is sensitive to the phase difference between V_{ub} and V_{cb} and thus to the angle γ. Most of the experimental methods to extract γ can be grouped in two categories: the D^0 and $\overline{D}^0$ decay into a CP eigenstate [5]; or the D^0 decays to a common flavor state, either through a Cabibbo-allowed or a doubly Cabibbo-suppressed mode [6]. The measurement of γ in both methods also requires the knowledge of r_B, the magnitude of the ratio of the amplitudes $\mathcal{A}(B^- \to \overline{D}^0 K^-)$ and $\mathcal{A}(B^- \to D^0 K^-)$ and of their relative strong phase δ_B, which can be obtained from data.
In this paper we report on a measurement of direct CP violation in $B^- \to D^{(*)0} K^-$ based on the analysis of the Dalitz distribution of the three-body decay $D^0 \to K_S \pi^- \pi^+$ [7]. The advantage of this method is that it involves the entire resonant substructure of the three-body decay, with Cabibbo-allowed and doubly Cabibbo-suppressed amplitudes interfering directly. It is therefore expected to have a higher statistical precision than the methods outlined above. Results of an analysis based on this procedure were reported by the Belle Collaboration in [8]. From the combination of the $B^- \to D^0 K^-$ and $B^- \to D^{*0} K^-$ mode they obtain the value $\gamma = 77^\circ {}^{+17^\circ}_{-19^\circ} \pm 13^\circ \pm 11^\circ$ where the first error is statistical, the second is experimental systematics and the third is model uncertainty. They also obtain a value of $r_B = 0.26^{+0.10}_{-0.14} \pm 0.03 \pm 0.04$ for $B^- \to D^0 K^-$ and $r_B^* = 0.20^{+0.19}_{-0.17} \pm 0.02 \pm 0.04$ for $B^- \to D^{*0} K^-$.

1.1 Analysis outline

The B^- and B^+ decay amplitudes for the $B^- \to D^{(*)0} K^-$ and $D^0 \to K_S \pi^- \pi^+$ decays can be written assuming no CP asymmetry in D decays as :

$$M_-(m_-^2, m_+^2) = |\mathcal{A}(B^- \to D^0 K^-)| \left[f(m_-^2, m_+^2) + r_B e^{i(\delta_B - \gamma)} \, f(m_+^2, m_-^2) \right], \quad (1)$$

$$M_+(m_-^2, m_+^2) = |\mathcal{A}(B^+ \to \overline{D}^0 K^+)| \left[f(m_+^2, m_-^2) + r_B e^{i(\delta_B + \gamma)} \, f(m_-^2, m_+^2) \right], \quad (2)$$

where m_-^2 and m_+^2 are the squared invariant masses of the $K_S \pi^-$ and $K_S \pi^+$ combinations respectively and $f(m_-^2, m_+^2)$ is the amplitude of the $D^0 \to K_S \pi^- \pi^+$ decay.

Given a known f, the bi-dimensional Dalitz (m_-^2, m_+^2) distributions for B^- and B^+ can be simultaneously fitted to $|M_-(m_-^2, m_+^2)|^2$ and $|M_+(m_-^2, m_+^2)|^2$ respectively. A maximum likelihood technique may be used to estimate r_B, δ_B, and γ. Since the measurement of γ arises from the interference in Eq. 1 and Eq. 2, the uncertainty in the knowledge of the complex form of $f(m_-^2, m_+^2)$ can lead to a systematic uncertainty. A model describing the $D^0 \to K_S \pi^- \pi^+$ decay in terms of two-body amplitudes has been assumed in this analysis. This model has been characterized using a high statistics flavor tagged D^0 sample ($D^{*+} \to D^0 \pi_s^+$), obtained from $e^+ e^- \to c\bar{c}$ events as described in Section 4.

A similar analysis is also performed using $B^- \to D^{*0}K^-$ decays, and γ is extracted along with the amplitude ratio r_B^* and strong phase difference δ_B^* taking into account the effective strong phase shift of π radians between the $D^{*0} \to D^0\pi^0$ and $D^{*0} \to D^0\gamma$ channels [9]. By convention δ_B^* is the strong phase of $D^{*0} \to D^0\pi^0$ decay mode.

2 THE *BABAR* DETECTOR AND DATASET

The analysis is based on a sample of 227 million $B\bar{B}$ pairs collected by the *BABAR* detector at the SLAC PEP-II e^+e^- asymmetric-energy storage ring. *BABAR* is a solenoidal detector optimized for the asymmetric-energy beams at PEP-II and is described in [10]. We summarize briefly the components that are crucial to this analysis. Charged-particle tracking is provided by a five-layer silicon vertex tracker (SVT) and a 40-layer drift chamber (DCH). In addition to providing precise spatial hits for tracking, the SVT and DCH also measure the ionization energy loss (dE/dx), which is used for particle identification of low-momentum charged particles. At higher momenta (p > 0.7 GeV/c) pions and kaons are identified by Cherenkov radiation detected in a ring-imaging device (DIRC). The typical separation between pions and kaons varies from 8σ at 2 GeV/c to 2.5σ at 4 GeV/c. Neutral cluster (photon) positions and energies are measured with an electromagnetic calorimeter (EMC) consisting of 6580 thallium-doped CsI crystals. Candidate π^0 mesons are reconstructed as pairs of photons, spatially separated in the EMC, with an invariant mass within 3σ of the π^0 mass. These systems are mounted inside a 1.5-T solenoidal super-conducting magnet.

3 EVENT SELECTION

We reconstruct the decays $B^- \to D^0K^-$ and $B^- \to D^{*0}K^-$ with $D^{*0} \to D^0\pi^0$, $D^0\gamma$. A larger sample of $B^- \to D^{(*)0}\pi^-$ is also reconstructed and is used as a control sample to determine the Probability Density Function (PDF) of the discriminating variables used in the likelihood fit for γ. D^0 candidates are reconstructed in the $K_S\pi^+\pi^-$ final state with the K_S reconstructed from pairs of oppositely charged pions with an invariant mass within 9 MeV/c^2 of the nominal K_S mass [11]. The two pions are constrained to originate from the same point. The angle α_{K_S} between the K_S line of flight and its momentum is required to satisfy the condition $\cos\alpha_{K_S}$ >0.99. D^0 candidates are selected by making all possible combinations of the K_S candidate and two oppositely charged pions with an invariant mass within 12 MeV/c^2 of the nominal D^0 mass.

The photon candidates for $D^{*0} \to D^0\gamma$ are reconstructed from clusters in the electromagnetic calorimeter with energy greater than 30 MeV and consistent with a photon shower profile. We select π^0 candidates from pairs of photon candidates and require $115 < m(\gamma\gamma) < 150$ MeV/c^2 and with total energy greater than 70 MeV. To improve the momentum resolution, the π^0 candidates are kinematically fitted with their mass constrained to the nominal π^0 mass. The D^0 candidates are combined with a low energy π^0 or γ. The D^{*0}-D^0 mass difference Δm is required to be within 2.5 (10) MeV/c^2 of the nominal Δm for $D^{*0} \to D^0\pi^0(\gamma)$.

A B^- candidate is obtained by combining a $D^{(*)0}$ candidate with a track ("bachelor" track) identified as a kaon as described in [10]. We improve the momentum resolution for the D^0 daughters by applying a kinematic mass constraint. For every B candidate two standard variables are defined,

the beam-energy-substituted mass $m_{\rm ES} \equiv \sqrt{(\frac{1}{2}s + \vec{p}_0 \cdot \vec{p}_B)^2/E_0^2 - p_B^2}$ and the energy difference $\Delta E \equiv E_B^* - \frac{1}{2}\sqrt{s}$, where the asterisk denotes the CM frame, s is the square of the total energy in the CM frame, p and E are, respectively, momentum and energy, and the subscripts 0 and B refer to $\Upsilon(4S)$ and $B^{\pm}$, respectively. The resolutions, evaluated on simulated signal events, are 2.6 MeV/c^2 and 17 MeV for m_{ES} and ΔE, respectively.

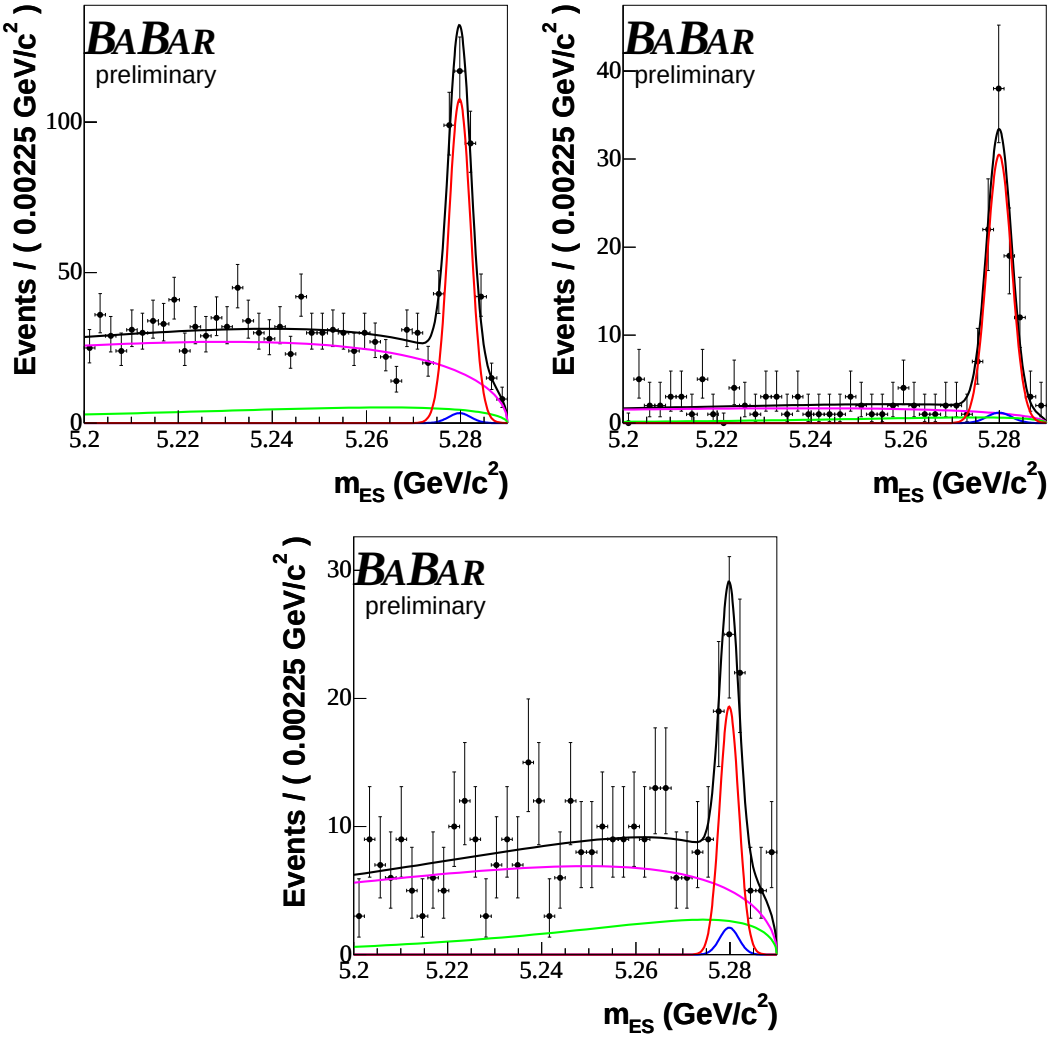

Figure 1: $B^- \to D^0 K^-$ (top left), $B^- \to D^{*0}(D^0\pi^0)K^-$ (top right) and $B^- \to D^{*0}(D^0\gamma)K^-$ (bottom) m_{ES} distribution in the ΔE region $[-30, 30]$ MeV in the sample of 211 million $B\bar{B}$ pairs. The signal contribution is shown in red, $B^- \to D^{*0}\pi^-$ in blue, generic $B\bar{B}$ in green, and continuum in magenta.

To distinguish between $B\overline{B}$ and continuum events the following topological variables are used: $\cos\theta_B^*$, where θ_B^* is the polar angle of the B candidate with respect to the beam axis in the CM frame; $L_0 = \sum_i p_i$ and $L_2 = \sum_i p_i \cos^2\theta_i$ calculated in the CM frame, where p_i and θ_i are the momenta and the angles of tracks and neutral clusters not used to reconstruct the B candidate with

respect to its thrust axis; $\cos\theta_T$, where θ_T is the angle in the CM frame between the thrust axes of the B candidate and of the rest of the event. B candidates are selected by requiring $|\cos\theta_T| < 0.8$. Under this condition a Fisher discriminant $\mathcal{F}$ is constructed from the variables discussed above. This Fisher discriminant is used in the likelihood fit to help distinguish between signal and continuum $e^+e^- \to q\bar{q}$ ($q = u, d, s, c$) events. The PDF of $\mathcal{F}$ is obtained for continuum events using m_{ES} sideband data. The $B^- \to D^{(*)0}\pi^-$ events are used to obtain the $\mathcal{F}$ PDF for $B\overline{B}$ and signal events.
Finally, the $B^- \to D^{(*)0}K^-$ sample events are required to satisfy $m_{ES} > 5.2$ GeV/c^2, $|\Delta E| < 30$ MeV. The $B^- \to D^{(*)0}\pi^-$ candidates are selected using criteria similar to those applied for $B^- \to D^{(*)0}K^-$ but requiring that the bachelor pion not be consistent with the kaon hypothesis. The overall reconstruction efficiencies are 18%, 4.3%, 8.1% for the D^0K^-, $D^{*0}(D^0\pi^0)K^-$, and $D^{*0}(D^0\gamma)K^-$ decay modes, respectively. Fig. 1 shows the m_{ES} distributions after all the selection criteria are applied.

4 DETERMINATION OF $D^0 \to K_S\pi^-\pi^+$ DECAY MODEL

The amplitude $f(m_\pm^2, m_\mp^2)$ has been constructed from a Dalitz analysis of a 97% pure flavor tagged D^0 sample obtained from 81496 $D^{*+} \to D^0\pi^+$ events corresponding to a luminosity of 91.5 fb^{-1} (Fig. 2). The Dalitz $(m_\pm^2, m_\mp^2)$ distribution (Fig. 3) is fitted in the context of the isobar formalism described in [12]. In this formalism the amplitude f can be written as a sum of two-body decay matrix elements and a non-resonant term according to the expression

$$f = a_{nr}e^{i\phi_{nr}} + \Sigma_r a_r e^{i\phi_r}\mathcal{A}_s(K_S\pi^-\pi^+|r). \quad (3)$$

Each term of the sum is parameterized with an amplitude and a phase. The factor $\mathcal{A}_s(K_S\pi^-\pi^+|r)$ gives the Lorentz invariant expression for the matrix element of a D^0 meson decaying into $K_S\pi^-\pi^+$ through an intermediate resonance r as a function of the position in the Dalitz plot. It is, in general, parameterized by a relativistic Breit-Wigner with a functional form dependent on the spin of the resonance. For the ρ a more complex parametrization is used as suggested in [13]. We fit the Dalitz distribution with a model consisting of 13 resonances leading to 17 two-body decay amplitudes and phases (Table 1). Of the 13 resonances eight involve a K_S plus a $\pi\pi$ resonance and the remaining five are made of a $(K_S\pi^-)$ resonance plus a π^+. We also include the corresponding doubly Cabibbo-suppressed amplitudes for most of the $(K_S\pi^-)$ π^+ decays. All the resonances considered in this model are well established except for the two scalar $\pi\pi$ resonances, σ_1 and σ_2, whose masses and widths are obtained from our sample. Those are introduced in order to obtain an acceptable fit to the data, but their existence as true, scalar particles is a matter outside the scope of the paper.

An unbinned maximum likelihood fit is performed to measure the amplitudes a_{nr}, a_r and the phases ϕ_{nr}, ϕ_r. The fit fraction for each decay channel is defined as the integral of a single component divided by the coherent sum of all components. The results of the fit are shown in Fig. 3. Amplitudes, phases and fit fractions as obtained by the likelihood fit are reported in Table 1.

We estimate the goodness of the fit for our model with a χ^2 fit using adaptive binning of the Dalitz plot. We obtain χ^2/d.o.f. = 3824/(3054-32) = 1.27.

To illustrate the region of the Dalitz plot most sensitive to γ measurement, we show in Fig. 4 the distribution of simulated $B^- \to D^0K^-$ events based on our Dalitz model, where each event is given a weight of $\frac{d^2\ln\mathcal{L}}{d^2\gamma}$ where $\mathcal{L}$ is the likelihood function described in the following section. The

Resonance	Amplitude	Phase (degrees)	Fraction (%)	Mass MeV/c^2	Width MeV/c^2	Functional form
$K^*(892)$	1.777 ± 0.018	131.0 ± 0.81	58.51	891.66	50.8	BW
$\rho^0(770)$	1 (fixed)	0(fixed)	22.33	775.8	146.4	GS
$K^*(892)$ DCS	0.1789 ± 0.0080	-44.0 ± 2.4	0.59	891.66	50.8	BW
$\omega(782)$	0.0391 ± 0.0016	114.8 ± 2.5	0.56	782.6	8.5	BW
$f_0(980)$	0.469 ± 0.011	213.4 ± 2.2	5.81	975	44	BW
$f_0(1370)$	2.32 ± 0.31	114.1 ± 4.4	3.39	1434	173	BW
$f_2(1270)$	0.915 ± 0.041	-22.0 ± 2.9	2.95	1275.4	185.1	BW
$K_0^*(1430)$	2.454 ± 0.074	-7.9 ± 2.0	8.37	1412	294	BW
$K_0^*(1430)$ DCS	0.350 ± 0.069	$-344. \pm 10.$	0.60	1412	294	BW
$K_2^*(1430)$	1.045 ± 0.045	-53.1 ± 2.6	2.70	1425.6	98.5	BW
$K_2^*(1430)$ DCS	0.074 ± 0.038	-98 ± 30	0.01	1425.6	98.5	BW
$K^*(1410)$	0.524 ± 0.073	-157 ± 10	0.39	1414	232	BW
$K^*(1680)$	0.99 ± 0.31	-144 ± 18	0.35	1717	322	BW
$\rho(1450)$	0.554 ± 0.097	$35 \pm 12.$	0.28	1406	455	GS
σ_1	1.346 ± 0.044	-177.5 ± 2.5	9.11	484 ± 9	383 ± 14	BW
σ_2	0.292 ± 0.025	-206.8 ± 4.3	0.98	1014 ± 7	88 ± 13	BW
Non resonant	3.41 ± 0.48	-233.9 ± 5.0	6.82	-	-	-

Table 1: Amplitudes, phases and fit fractions of the different components obtained from the likelihood fit of the $D^0 \to K_S\pi^-\pi^+$ Dalitz distribution in $D^{*\pm} \to D^0\pi_s^\pm$ data. Masses and widths of all resonances except σ_1 and σ_2 are taken from [11]. The abbreviations BW and GS stand for relativistic Breit-Wigner and Gounaris-Sakurai [13] respectively. The total fit fraction is 1.24.

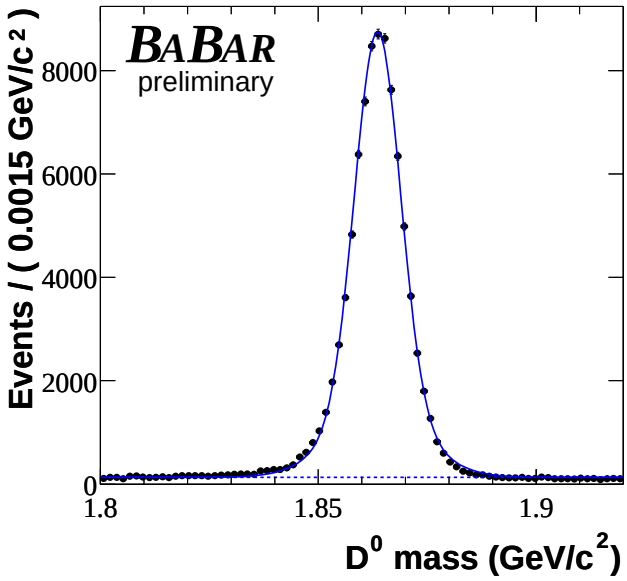

Figure 2: The $K_S\pi^-\pi^+$ invariant mass distribution in the flavor tagged D^* sample.

regions of interference between doubly Cabibbo suppressed and Cabibbo allowed decays and CP eigenstate decays exhibit the highest sensitivity to γ.

5 CP FIT TO $B \to D^{(*)0}K$ SAMPLES

A maximum likelihood fit (CP fit) is performed on the $B^- \to D^{(*)0}K^-$ samples to extract simultaneously the CP violation parameters γ, $\delta_B^{(*)}$, and $r_B^{(*)}$ and the signal and background yields. The likelihood for each candidate j is obtained by summing the product of the event yield N_i and the probability $\mathcal{P}_i$ over the signal and the three background hypotheses. The extended likelihood function is

$$\mathcal{L} = \exp\left(-\sum_i N_i\right) \prod_j \left[\sum_i N_i \mathcal{P}_i(\vec{x}_j)\mathcal{P}_i^{\rm Dal}(m_+^2, m_-^2)\right]. \quad (4)$$

The probabilities $\mathcal{P}_i$ are evaluated as the product of the PDFs for each of the independent variables $\vec{x}_j = \{m_{\rm ES}, \Delta E, \mathcal{F}\}$. $\mathcal{P}_i^{\rm Dal}(m_+^2, m_-^2)$ is the PDF for the Dalitz distribution for the i^{th} category. The categories in the fit are signal $B^- \to D^{(*)0}K^-$, the continuum background, $B\bar{B}$ background, and $B^- \to D^{*0}\pi^-$ and are shown in Fig. 1. The m_{ES} and ΔE distributions for signal events are described by a Gaussian. The Fisher PDF is parametrized with a double Gaussian function. The signal PDF parameters are determined from the $B^- \to D^{(*)0}\pi^-$ control sample.

5.1 Background Composition

The numbers of events for the various background components in the $B^- \to D^{(*)0}K^-$ samples are summarized in Table 2. The dominant background contribution is from the random combination of a real or fake $D^{(*)0}$ meson with a charged track in continuum events or other $B\bar{B}$ decays. The combinatorial background in the m_{ES} distribution is described by a threshold function [14]

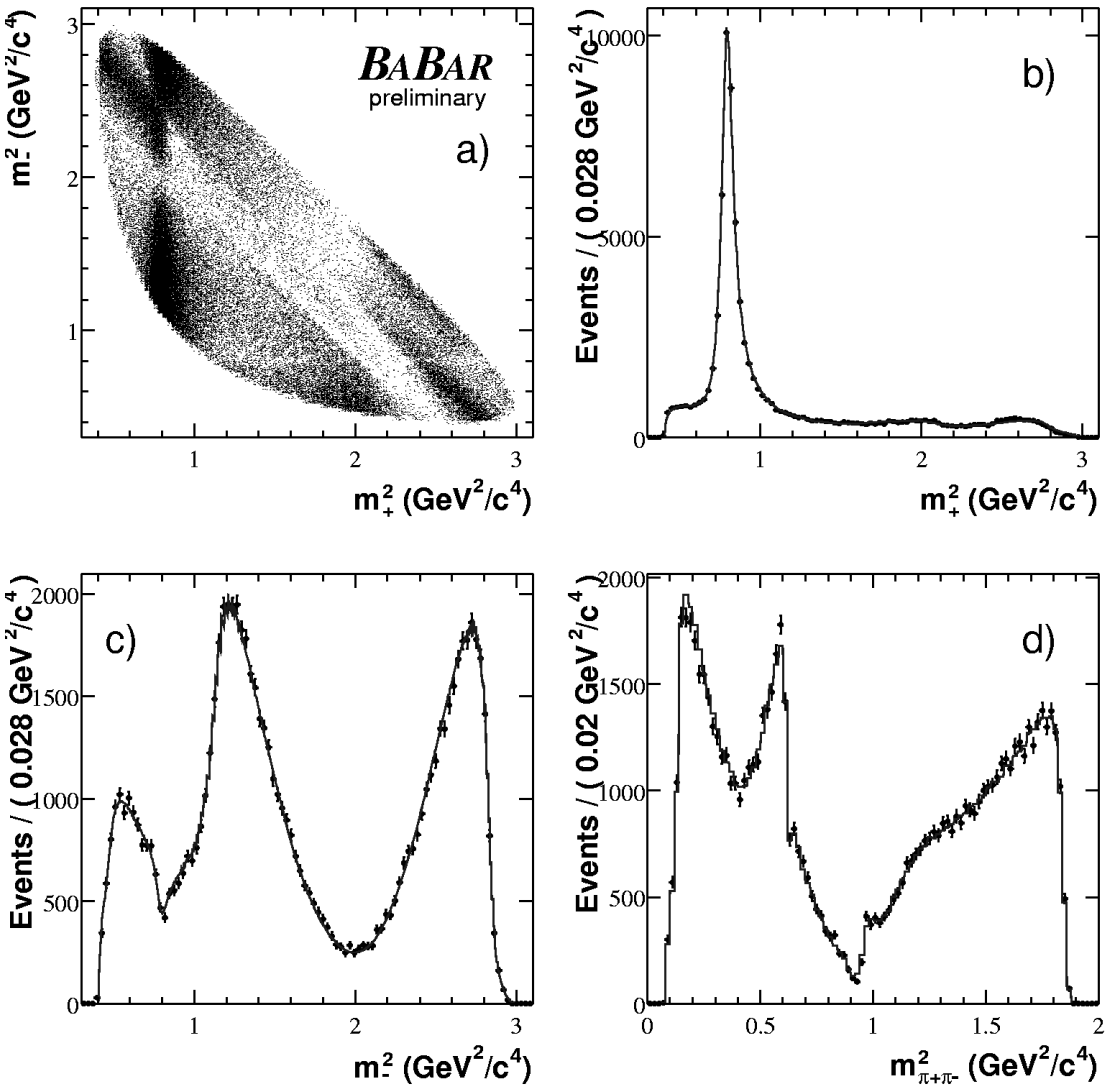

Figure 3: (a) The $\overline{D}^0 \to K_S\pi^+\pi^-$ Dalitz distribution from the $D^{*+} \to D^0\pi^+$ events. Projections on (b) m_+^2, (c) m_-^2, and (d) $m^2(\pi^+\pi^-)$ are shown. The result of the fit is superimposed as a solid line.

whose free parameter ξ is determined from the $B^- \to D^{(*)0}\pi^-$ data sample. The shape of the combinatorial background m_{ES} distribution in generic $B\bar{B}$ decays is taken from simulated events. The ΔE distribution is described by a straight line whose slope is extracted from a fit to the $B^- \to D^{(*)0}\pi^-$ sample. The PDF of the Fisher distribution for continuum events is determined from the m_{ES} sideband in the same data sample. The Fisher PDF for $B\bar{B}$ events is assumed to be the same as that for the signal.

An important class of background events arises from continuum where a real D^0 is produced back-to-back with a kaon. Depending on the flavor-charge correlation this background can mimic either the $b \to c$ or the $b \to u$ signal component. In the likelihood function we take this effect

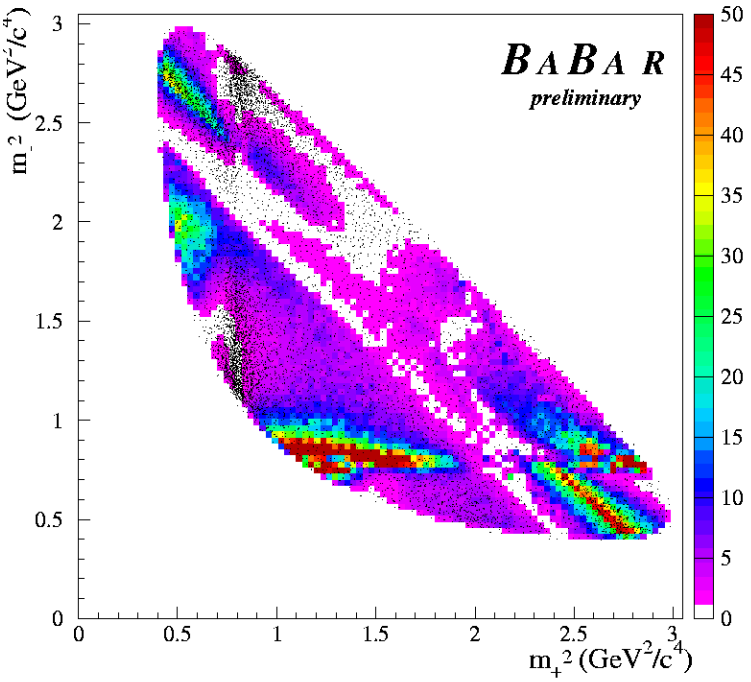

Figure 4: $\overline{D}^0 \to K_S\pi^+\pi^-$ Dalitz distribution of simulated ($B^+ \to \overline{D}^0 K^+$) events. Each event is given a weight $\frac{d^2 \ln \mathcal{L}}{d^2\gamma}$. The black points represent the same events with weight equal to unity.

into account with two parameters, the fraction f_{D^0} of background events with a real D^0 and the parameter R, the fraction of background events with a real D^0 associated with an oppositely flavored kaon (same charge correlation as the $b \to u$ signal component).

The fraction of real D^0 from continuum events has been evaluated in events satisfying m_{ES} < 5.272 GeV/c^2 after removing the requirement on the D^0 mass. The fraction R of background events with a genuine D^0 associated with a negatively charged kaon is obtained from simulated events. The values of f_{D^0} and R for continuum $q\bar{q}$ are summarized in Table 3. The fraction of events with a real D^0 in generic $B\overline{B}$ events is found to be few percent.

A small background originates from $B^- \to D^{(*)0}\pi^-$ where the bachelor pion is misidentified as a kaon. These events have the same m_{ES} distribution as signal but can be distinguished using their ΔE information.

5.2 Likelihood fit on control samples

We test our CP fit procedure on two high statistics control samples: $D^{*+} \to D^0\pi^+$ from $c\bar{c}$ continuum events and $B^- \to D^{(*)0}\pi^-$. The $D^{*+} \to D^0\pi^+$ sample mimics a $B^- \to D^0K^-$ sample with $r_B = 0$. The $B^- \to D^0\pi^-$ sample is similar to $B^- \to D^0K^-$, but its r_B is expected to be approximately 0.007 [15]. In the CP fit to $D^{*+} \to D^0\pi^+$ we obtain $r_B = (-5.2 \pm 5.2) \times 10^{-3}$. In the $B^- \to D^0\pi^-$ we obtain $r_B = (1.8 \pm 1.5) \times 10^{-2}$, $\gamma = (18 \pm 45)^\circ$, $\delta_B = (246 \pm 43)^\circ$ and in $B^- \to D^{*0}\pi^-$ we find $r_B^* = (4.6 \pm 2.1) \times 10^{-2}$, $\gamma = (90 \pm 35)^\circ$, $\delta_B^* = (117 \pm 35)^\circ$. The results

Background components	D^0K^-	$(D^0\pi^0)\ K^-$	$(D^0\gamma)K^-$
Continuum $q\bar{q}$	125 ± 6	9 ± 2	38 ± 3
$B\bar{B}$	28 ± 7	4 ± 2	14 ± 5
$D\pi$	9 ± 8	0 ± 5	6 ± 4

Table 2: Estimates of the numbers of background events in the $m_{ES} > 5.272$ GeV/c^2 region from the fit to data in the full m_{ES} region for the $B^- \to D^0K^-$, $B^- \to D^{*0}(D^0\pi^0)K^-$, and $B^- \to D^{*0}(D^0\gamma)K^-$ samples.

$q\bar{q}$ background parameters	D^0K^-	$(D^0\pi^0)K^-$	$(D^0\gamma)K^-$
f_{D^0}	0.27 ± 0.06	0.27 ± 0.13	0.13 ± 0.02
R	0.21 ± 0.03	0.23 ± 0.11	0.16 ± 0.06

Table 3: $q\bar{q}$ background parameters for the $B^- \to D^0K^-$, $B^- \to D^{*0}(D^0\pi^0)K^-$, and $B^- \to D^{*0}(D^0\gamma)K^-$ samples.

obtained are consistent with the expectations of Monte Carlo experiments.

5.3 Likelihood fit on $B^- \to D^{(*)0}K^-$ sample

In the sample of 227 million $B\bar{B}$ events we obtain the following signal yields

$$\begin{aligned} N(B^- \to D^0K^-) &= 282 \pm 20, \\ N(B^- \to D^{*0}(D^0\pi^0)K^-) &= 89 \pm 11, \\ N(B^- \to D^{*0}(D^0\gamma)K^-) &= 44 \pm 8, \end{aligned} \tag{5}$$

in agreement with our expectation from simulation and measured branching ratios. We obtain the following CP parameters from the fit for $B^- \to D^0K^-$, $r_B = 0.117 \pm 0.053$, $\delta_B = (109 \pm 28)^\circ$, and $\gamma = (66 \pm 28)^\circ$ and for $B^- \to D^{*0}K^-$, $r_B^* = 0.167 \pm 0.065$, $\delta_B^* = (294 \pm 28)^\circ$, and $\gamma = (68 \pm 29)^\circ$. These errors are estimated with a Gaussian assumption for the likelihood. However, for this small sample, these low r_B and r_B^* fitted values lead to a non-Gaussian behavior of the likelihood function as shown in Fig. 5, necessitating a different approach, described next, in the computation of the confidence intervals for r_B, γ and δ_B. Fig. 6 shows for r_B values generated in the $[0.0, 0.3]$ range the r_B values obtained in fits to Monte Carlo experiments of the same size as data. While the CP fit is linear for large values of r_B, it is not sensitive to r_B values below 0.1. This problem did not exist for the larger $D^{*+} \to D^0\pi^+$ and $B^- \to D^{(*)0}\pi^-$ samples as we have verified using Monte Carlo simulation.

In Fig. 7 and Fig. 8 we show the Dalitz distribution and the m_+^2 and m_-^2 projections for events with $m_{ES} > 5.272$ GeV/c^2 for $B^- \to D^0K^-$ and $B^- \to D^{*0}K^-$ respectively. B^+ and B^- candidates distributions are separately shown with the total PDF superimposed.

5.4 Confidence intervals of the CP parameters

We evaluate the likelihood function $\mathcal{L}$ (r_B, γ, δ_B) after fixing all parameters except (r_B, γ, δ_B) which are varied in their range of definition, [0,1], [-π,π], and [0,2π], respectively. We then estimate

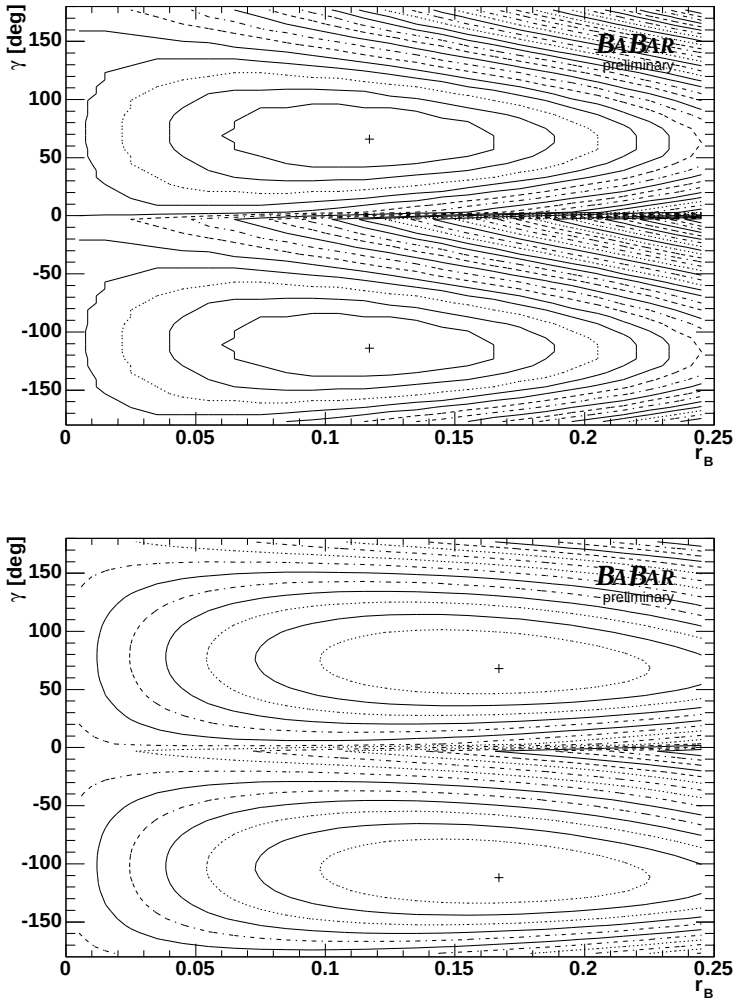

Figure 5: $\ln \mathcal{L}$ contour plots in γ versus r_B in $B^- \to D^0 K^-$ (top) and $B^- \to D^{*0} K^-$ (bottom). δ_B is fixed to the value obtained from the fit. Each contour represent a $\ln \mathcal{L}$ variation of 0.5.

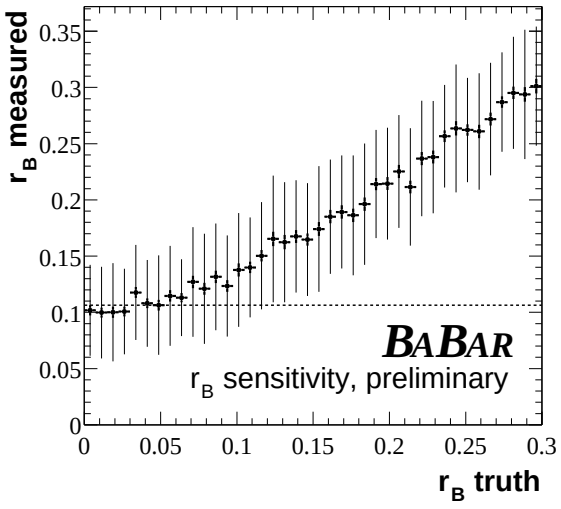

Figure 6: r_B values obtained in the likelihood fit versus generated r_B values in Monte Carlo $B^- \to D^0 K^-$ experiments. The error bars represent the RMS of the r_B values returned by the fit. The dashed horizontal line indicates the r_B value (0.106) found in data.

the confidence region for the CP parameters using a Bayesian technique. This implies a choice of a priori distribution. For this preliminary result we arbitrarily assume a uniform a priori distribution for each of the CP parameters r_B,γ and δ_B.

In γ-r_B space we define a two-dimensional confidence region $\mathcal{D}(\mathcal{C})$ corresponding to a given confidence level $\mathcal{C}$

$$\frac{\int_{D(\mathcal{C})} dr_B d\gamma \int_0^{2\pi} d\delta_B \mathcal{L}(r_B,\gamma,\delta_B)}{\int_0^1 dr_B \int_{-\pi}^{\pi} d\gamma \int_0^{2\pi} d\delta_B \mathcal{L}(r_B,\gamma,\delta_B)} = \mathcal{C}$$

We uniquely define $D(\mathcal{C})$ by requiring that the likelihood value at any point on the boundary of $\mathcal{D}$ be the same and integrating over all likelihood values larger than the value at the boundary.

Similarly we define one dimensional confidence intervals $I(\mathcal{C})$ corresponding to a confidence level $\mathcal{C}$. For example, the interval for r_B is defined as

$$\frac{\int_{I(\mathcal{C})} dr_B \int_{-\pi}^{+\pi} d\gamma \int_0^{2\pi} d\delta_B \mathcal{L}(r_B,\gamma,\delta_B)}{\int_0^1 dr_B \int_{-\pi}^{\pi} d\gamma \int_0^{2\pi} d\delta_B \mathcal{L}(r_B,\gamma,\delta_B)\, dr_B} = \mathcal{C}$$

The two dimensional confidence regions $\mathcal{D}(\mathcal{C})$ in γ versus r_B and γ versus r_B^* are shown in Fig. 9. The red (dark) and yellow (light) regions correspond to the 68% and 95% confidence levels respectively. The likelihood distributions for r_B, γ, and δ_B obtained by integrating $\mathcal{L}(r_B, \gamma, \delta_B)$ over the other two variables are shown in Figs. 10, 11 and 12 respectively. The 68% and 95% confidence intervals are shown in red (dark) and yellow (light) respectively. The intervals for γ and δ_B are disjoint as a consequence of the $\gamma \to \gamma \pm \pi$ and $\delta_B \to \delta_B \pm \pi$ ambiguities.

5.5 Constraints on r_B, δ_B and γ

From the procedure above we obtain Bayesian 68% confidence intervals. We quote as the central values for γ and δ_B the average values weighted by the likelihood distribution. The errors associated

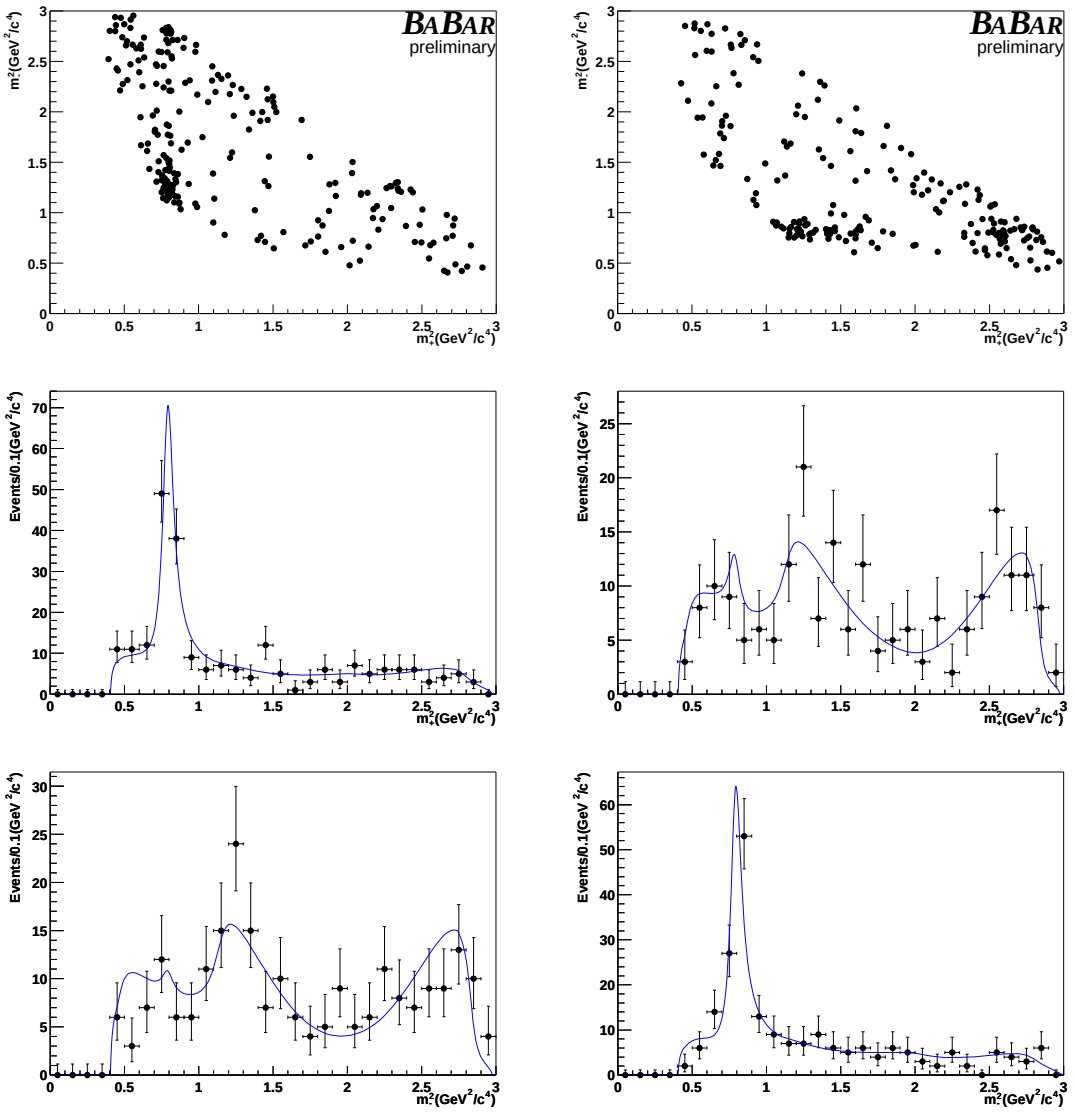

Figure 7: Dalitz distribution (first row) from the $B^- \to D^0 K^-$ events with $m_{ES} > 5.272$ GeV/c^2. Projections on m_+^2 (second row) and m_-^2 (third row) are shown with the result of the fit superimposed. In the left column B^+ candidates are shown, in the right B^- candidates.

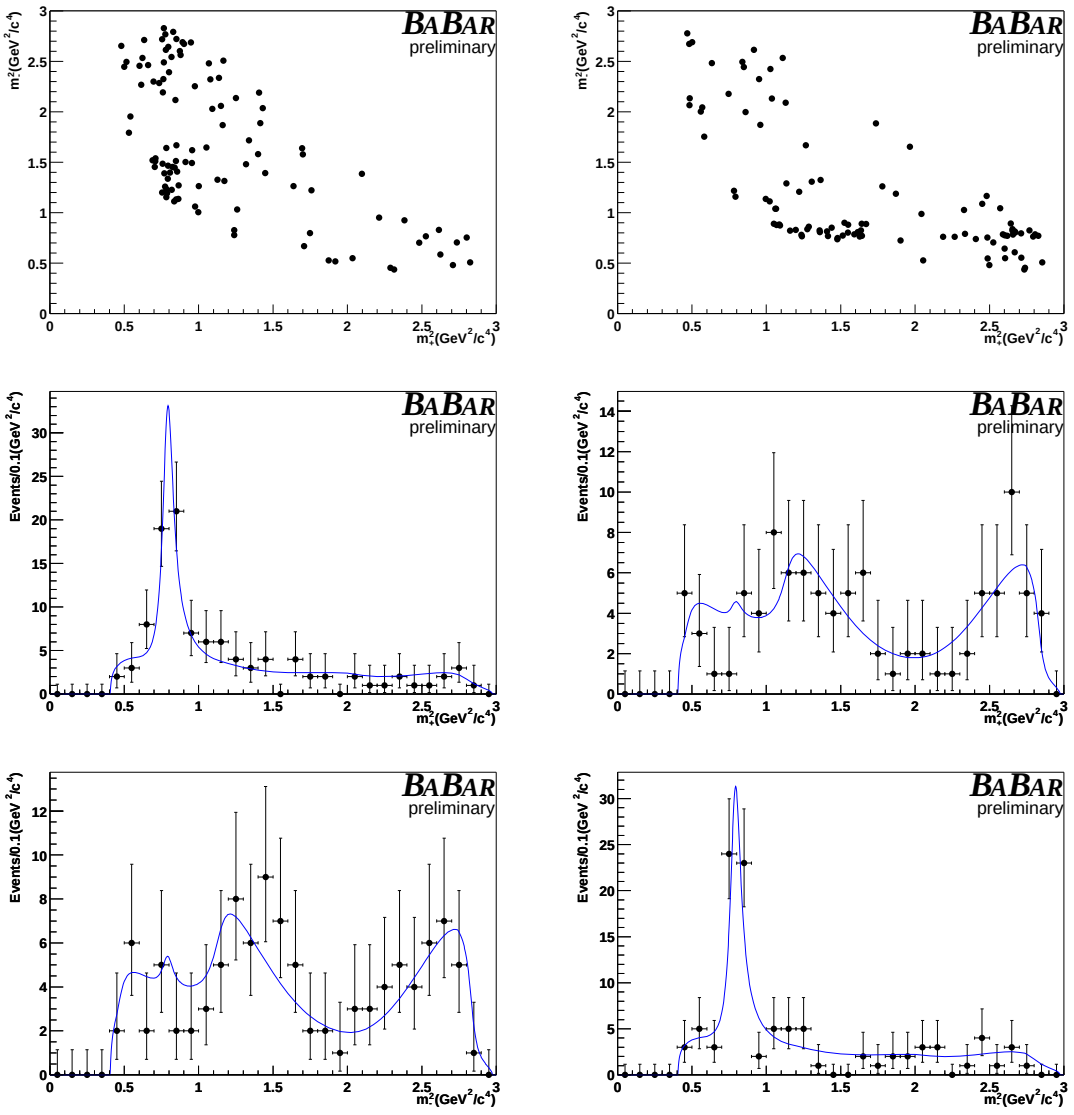

Figure 8: Dalitz distribution (first row) from the $B^- \to D^{*0}K^-$ events with $m_{ES} > 5.272$ GeV/c^2. Projections on m_+^2 (second row) and m_-^2 (third row) are shown with the result of the fit superimposed. In the left column B^+ candidates are shown, in the right B^- candidates.

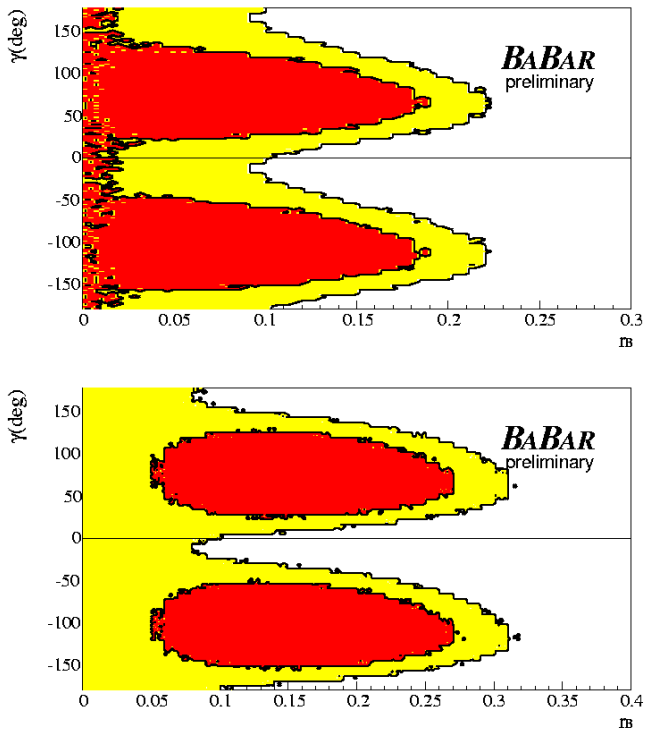

Figure 9: Bayesian confidence regions for γ versus r_B (top) and r_B^* (bottom) for the $B^- \to D^0 K^-$ and $B^- \to D^{*0} K^-$ samples respectively. The red (dark) region corresponds to the 68% confidence level region, the yellow (light) region to the 95% C.L. region

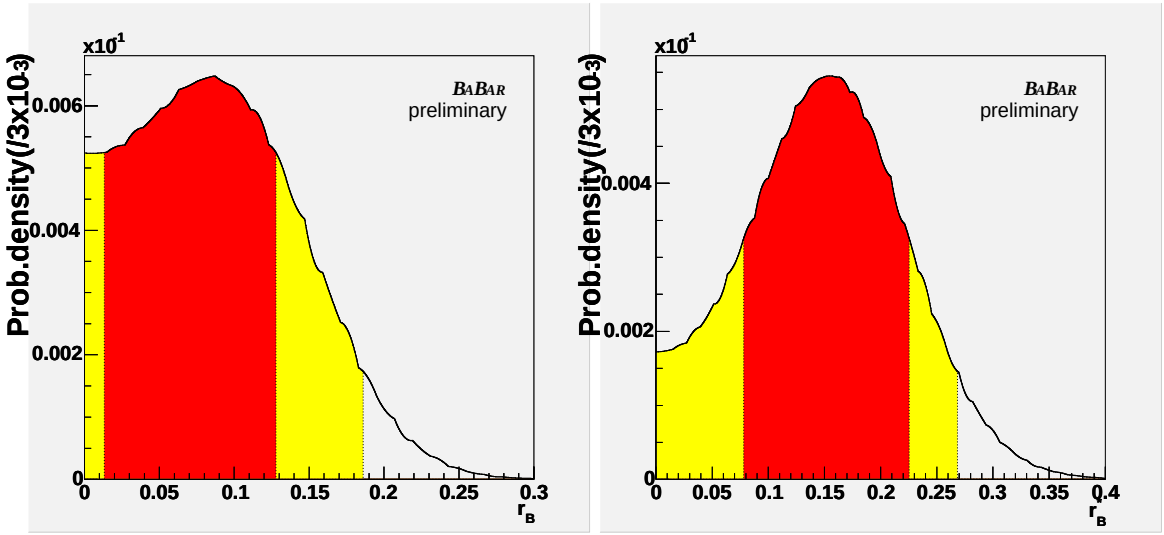

Figure 10: Probability density function for r_B (left) and r_B^* (right). The red (dark) region corresponds to the Bayesian 68% confidence level region, the yellow (light) region to the 95% C.L. region.

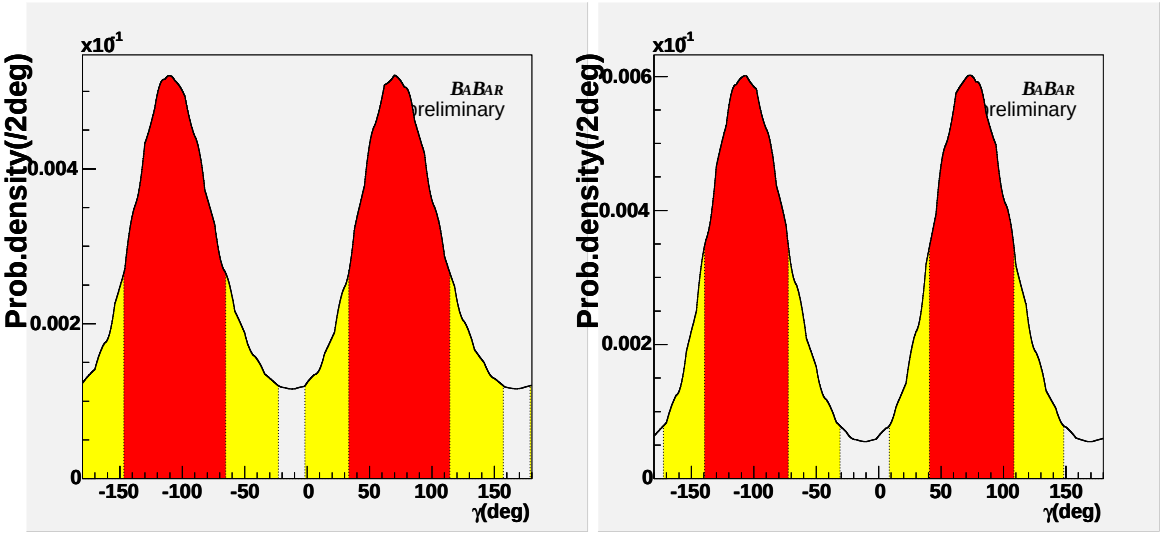

Figure 11: Probability density function for γ in $B^- \to D^0 K^-$ (left) and $B^- \to D^{*0} K^-$ (right) sample . The red (dark) region corresponds to the Bayesian 68% confidence interval region, the yellow (light) region to the 95% C.L. region. The intervals for γ are disjoint as a consequence of the $\gamma \to \gamma \pm \pi$ and $\delta_B \to \delta_B \pm \pi$ ambiguities.

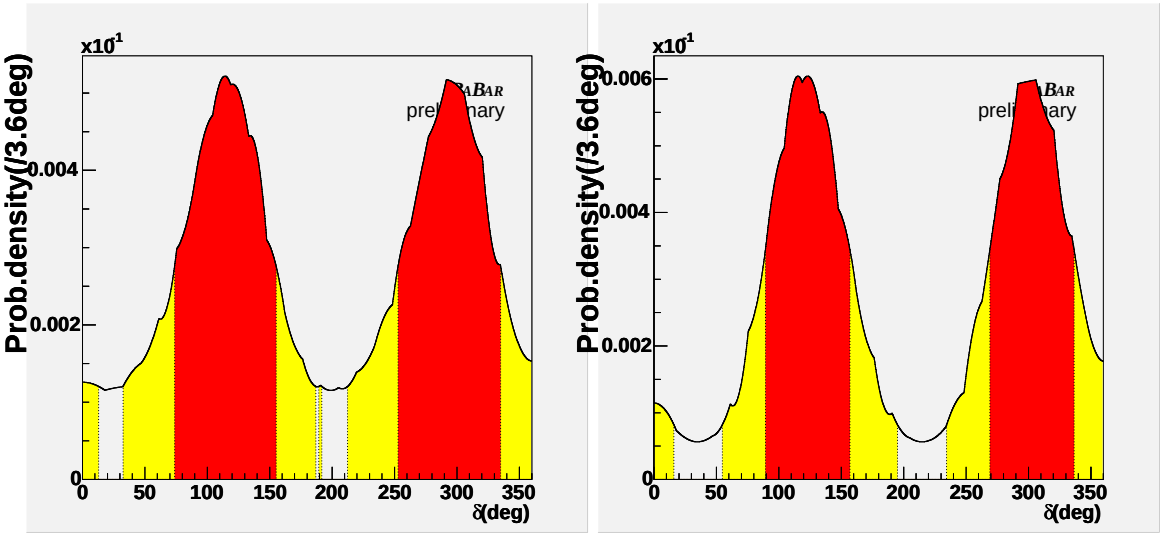

Figure 12: Probability density function for δ_B in $B^- \to D^0 K^-$ (left) and $B^- \to D^{*0} K^-$ (right) sample. The red (dark) region corresponds to the Bayesian 68% confidence interval region, the yellow (light) region to the 95% C.L. region. The intervals for δ_B are disjoint as a consequence of the $\gamma \to \gamma \pm \pi$ and $\delta_B \to \delta_B \pm \pi$ ambiguities.

with the central values are defined by the boundaries of the 68% confidence interval. We obtain $r_B = 0.087 \pm^{+0.041}_{-0.074}$, $\delta_B = 114^\circ \pm 41^\circ (294^\circ \pm 41^\circ)$, $\gamma = 70^\circ \pm 44^\circ (-110^\circ \pm 44^\circ)$ for $B^- \to D^0 K^-$ and $r_B^* = 0.155^{+0.070}_{-0.077}$, $\delta_B^* = 303^\circ \pm 34^\circ (123^\circ \pm 34^\circ)$, $\gamma = 73^\circ \pm 35^\circ (-107^\circ \pm 35^\circ)$ for $B^- \to D^{*0} K^-$. We constrain r_B to be < 0.16 at 90% confidence level.

As illustrated in Figs. 5 and 13, the data have no sensitivity to γ and δ_B for small values of r_B. Those values are not excluded by our data.

We construct a combined likelihood function from the product of the individual likelihoods for $B^- \to D^0 K^-$ and $B^- \to D^{*0} K^-$ and we repeat the procedure outlined above. From this we obtain $\gamma = 70^\circ \pm 26^\circ$ $(-110^\circ \pm 26^\circ)$. Fig. 14 shows the γ likelihood distribution.

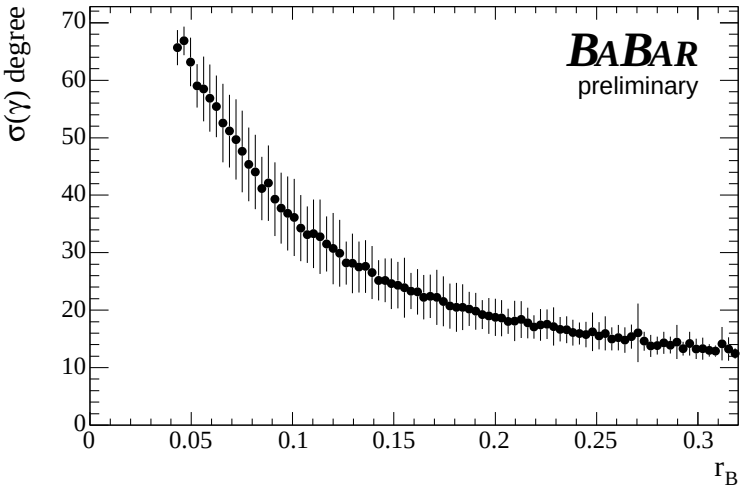

Figure 13: Statistical uncertainty in Gaussian hypothesis for γ as a function of the value of r_B obtained by the likelihood fit in Monte Carlo experiments.

6 SYSTEMATIC UNCERTAINTIES

The principal systematic uncertainty on the measurement of γ comes from the choice of the model used to describe $D^0 \to K_S \pi^- \pi^+$ decay. We evaluate this uncertainty by considering alternative models. For each model we generate events and fit both the alternative model and the nominal model (defined in Section 4) to these events. We quantify this uncertainty using the differences in the fitted values for r_B, δ_B and γ. For models where the $\rho(1450)$, the $K^*(1680)$ and/or the doubly Cabibbo suppressed $K_0^*(1430)$ and $K_2^*(1430)$ are removed or a different description of resonances is used, the χ^2 of the fit is not significantly different from that of the nominal model. For these models the biases on γ and r_B are negligible and the RMS of the distribution of the differences is at most 1° and 0.002 for γ and r_B respectively. As an extreme we consider a model without the σ_1 and/or σ_2 scalar, or the CLEO Model [12]. Fits to these models result in a significantly larger χ^2 than that of the nominal model. To illustrate the magnitude of this variation Fig. 15 shows the result of a fit with the CLEO model. For these extreme models the biases for CP parameters are still small. The RMS of the differences for γ and r_B are approximately 10° and 0.02 respectively. We conservatively assign $\sigma_\gamma, \sigma_{\delta_B} = 10^\circ$ and $\sigma_{r_B} = 0.02$ as systematic uncertainties associated with

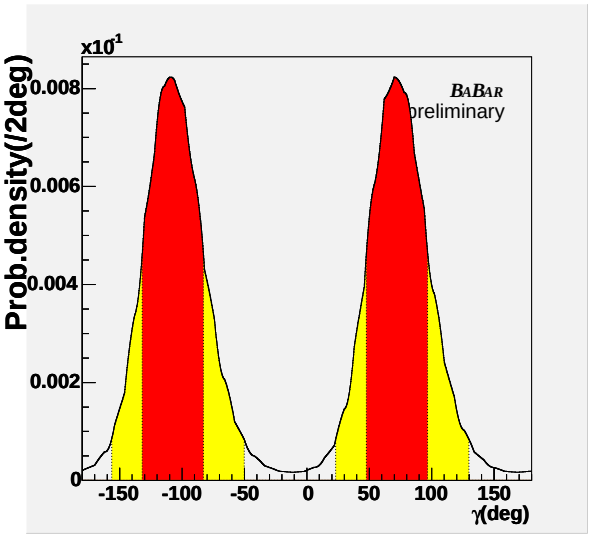

Figure 14: Probability density function for γ from the combined samples.The red (dark) region corresponds to the Bayesian 68% confidence interval region, the yellow (light) region to the 95% C.L. region.

the Dalitz model.

The summary of the estimates of other systematic uncertainties is given in Table 4. The most important effect is due to the uncertainties on the knowledge of the Dalitz distribution of background events and of the m_{ES}, ΔE, and $\mathcal{F}$ PDF parameters for both background and signal. Uncertainties in the efficiency variation across the Dalitz distribution are estimated. The statistical uncertainty on the amplitude and phases of the nominal Dalitz model also contributes significantly to the systematic uncertainties on the CP parameters.

	$B^- \to D^0 K^-$			$B^- \to D^{*0} K^-$		
Source	r_B	γ	δ_B	r_B^*	γ	δ_B^*
Combinatorial background Dalitz shape	0.008	6.7°	3.3°	0.010	2.9°	5.1°
m_{ES}, ΔE, $\mathcal{F}$ PDF shapes	0.007	5.4°	4.2°	0.025	1.8°	8.2°
R	0.018	3.1°	3.0°	0.018	3.1°	3.0°
Efficiency	0.004	3.0°	2.7°	0.005	3.0°	2.8°
Dalitz amplitude and phase uncertainties	0.004	1.6°	4.7°	0.014	6.1°	8.8°
Total	0.022	9.8°	8.3°	0.036	8.2°	13.8°

Table 4: Summary of the contributions to the systematic errors on r_B, γ and δ_B.

7 RESULTS AND SUMMARY

We report preliminary results of the measurement of r_B and of the angle γ using the B^- meson decays into $D^0 K^-$ and $D^{*0} K^-$ with a technique based on the Dalitz analysis of the $D^0 \to K_S \pi^- \pi^+$ three-body decay. From 227 million $B\bar{B}$ pairs collected by the *BABAR* detector, we reconstruct

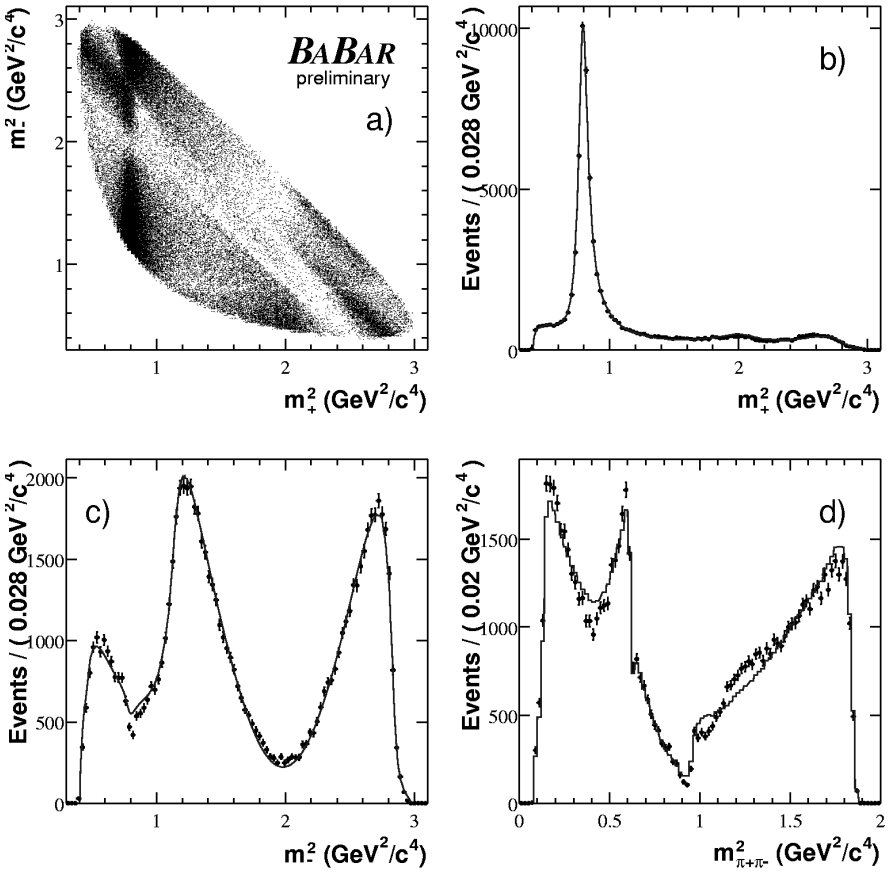

Figure 15: CLEO model fit: a) the $\overline{D}^0 \to K_S\pi^+\pi^-$ Dalitz distribution from the $D^{*-} \to \overline{D}^0\pi^-$. Projection on (b) m_+^2, (c) m_-^2 and (d) $m^2(\pi^+\pi^-)$ are shown. The result of the fit is superimposed and it is used to estimate the uncertainty due to the Dalitz model.

282 ± 20 $B^- \to D^0K^-$, 89 ± 11 $B^- \to D^{*0}K^-$, $D^{*0} \to D^0\pi^0$ and 44 ± 8 $B^- \to D^{*0}K^-$, $D^{*0} \to D^0\gamma$ signal events.

Values of the ratio of $b \to u$ and $b \to c$ amplitudes for the processes $B^- \to D^0K^-$ and $B^- \to D^{*0}K^-$ at the small end of our measurements allow no determination of γ at this statistical level. Accounting for systematic uncertainties, we constrain these ratios to be $r_B < 0.19$ at 90% confidence level and $r_B^* = 0.155^{+0.070}_{-0.077} \pm 0.040 \pm 0.020$. The relative phases between these two amplitudes are $\delta_B = 114^\circ \pm 41^\circ \pm 8^\circ \pm 10^\circ (294^\circ \pm 41^\circ \pm 8^\circ \pm 10^\circ)$ and $\delta_B^* = 303^\circ \pm 34^\circ \pm 14^\circ \pm 10^\circ (123^\circ \pm 34^\circ \pm 14^\circ \pm 10^\circ)$. The first error is statistical, the second error accounts for experimental uncertainties and the third error reflects the Dalitz model uncertainty. By combining the information from the two samples we obtain $\gamma = 70^\circ \pm 26^\circ \pm 10^\circ \pm 10^\circ$ $(-110^\circ \pm 26^\circ \pm 10^\circ \pm 10^\circ)$. For this preliminary result we have quoted confidence intervals obtained with a Bayesian technique assuming a uniform prior in r_B, γ and δ_B.

8 ACKNOWLEDGMENTS

We are grateful for the extraordinary contributions of our PEP-II colleagues in achieving the excellent luminosity and machine conditions that have made this work possible. The success of this project also relies critically on the expertise and dedication of the computing organizations that support *BABAR*. The collaborating institutions wish to thank SLAC for its support and the kind hospitality extended to them. This work is supported by the US Department of Energy and National Science Foundation, the Natural Sciences and Engineering Research Council (Canada), Institute of High Energy Physics (China), the Commissariat à l'Energie Atomique and Institut National de Physique Nucléaire et de Physique des Particules (France), the Bundesministerium für Bildung und Forschung and Deutsche Forschungsgemeinschaft (Germany), the Istituto Nazionale di Fisica Nucleare (Italy), the Foundation for Fundamental Research on Matter (The Netherlands), the Research Council of Norway, the Ministry of Science and Technology of the Russian Federation, and the Particle Physics and Astronomy Research Council (United Kingdom). Individuals have received support from CONACyT (Mexico), the A. P. Sloan Foundation, the Research Corporation, and the Alexander von Humboldt Foundation.

References

[1] *BABAR* Collaboration, B. Aubert *et al.*, Phys. Rev. Lett. **89**, 201802 (2002); Belle Collaboration, K. Abe *et al.* Phys. Rev. **D66**, 071102 (2002).

[2] N. Cabibbo, Phys. Rev. Lett. **10**, 531 (1963); M. Kobayashi and T. Maskawa, Prog. Theor. Phys. **49**, 652 (1973).

[3] L.Wolfenstein, Phys. Rev. Lett. **51** 1945 (1983).

[4] Reference to the charge-conjugate state is implied here and throughout the text unless otherwise stated.

[5] M. Gronau and D. London, Phys. Lett. **B253**, 483 (1991); M. Gronau and D. Wyler, Phys. Lett.**B265**, 172 (1991).

[6] I. Dunietz, Phys. Lett. **B270**, 75 (1991); I. Dunietz, Z. Phys. **C56**, 129 (1992); D. Atwood, G. Eilam, M. Gronau and A. Soni, Phys. Lett. **B341**, 372 (1995); D. Atwood, I. Dunietz and A. Soni, Phys. Rev. Lett. **78**, 3257 (1997).

[7] A. Giri, Yu. Grossman, A. Soffer and J. Zupan, Phys. Rev. **D68**, 054018 (2003).

[8] A. Poluektov *et al.* [Belle Collaboration], arXiv:hep-ex/0406067.

[9] A. Bondar and T. Gershon, arXiv:hep-ph/0409281.

[10] *BABAR* Collaboration, B. Aubert *et al.*, Nucl. Instr. Meth. **A 479**, 1 (2002).

[11] Particle Data Group, S. Eidelman *et al.*, Phys. Lett. **B592**, 1 (2004)

[12] S. Kopp et al. (CLEO Coll.) Phys. Rev. **D63** 092001 (2001); H. Muramatsu et al. (CLEO Coll.) Phys. Rev. Lett. **89** 251802 (2002); Erratum-ibid: **90** 059901 (2003).

[13] G.J. Gounaris and J.J. Sakurai, Phys. Rev. Lett. **21** 244, (1968);

[14] $\frac{dN}{dm_{ES}} = N \cdot m_{\rm ES} \cdot \sqrt{1-x^2} \cdot \exp\left(-\xi \cdot (1-x^2)\right)$ where $x = 2m_{\rm ES}/\sqrt{s}$ and the parameter ξ is determined from a fit. ARGUS Collaboration, H. Albrecht *et al.*, Z. Phys. C **48**, 543 (1990).

[15] r_B in $B^- \to D^{(*)0}\pi^-$ can be roughly estimated as $\frac{|V_{ub}^* V_{cd}|}{|V_{cb}^* V_{ud}|} \cdot \frac{1}{3} \sim 0.007$ where $\frac{1}{3}$ accounts for the color suppression.